JACS
JOURNAL OF THE AMERICAN CHEMICAL SOCIETY
Article
pubs.acs.org/JACS

Probing Adsorption Interactions in Metal–Organic Frameworks using X-ray Spectroscopy

Walter S. Drisdell,[†] Roberta Poloni,[†,‡,§,∥] Thomas M. McDonald,[†,§] Jeffrey R. Long,[†,§] Berend Smit,[‡,§] Jeffrey B. Neaton,[†] David Prendergast,[†] and Jeffrey B. Kortright*[,†]

[†]Materials Sciences Division, Lawrence Berkeley National Laboratory, Berkeley, California 94720, United States
[‡]Department of Chemical and Biomolecular Engineering, University of California, Berkeley, California 94720-1460, United States
[§]Department of Chemistry, University of California, Berkeley, California 94720-1460, United States
[∥]Laboratoire de Science et Ingénierie des Matériaux et Procédés (SIMaP), UMR CNRS 5266, Grenoble-INP, BP 75, 38402 Saint Martin d'Hères Cedex, France

Supporting Information

ABSTRACT: We explore the local electronic signatures of molecular adsorption at coordinatively unsaturated binding sites in the metal–organic framework Mg-MOF-74 using X-ray spectroscopy and first-principles calculations. In situ measurements at the Mg K-edge reveal distinct pre-edge absorption features associated with the unique, open coordination of the Mg sites which are suppressed upon adsorption of CO_2 and *N*,*N*′-dimethylformamide. Density functional theory shows that these spectral changes arise from modifications of local symmetry around the Mg sites upon gas uptake and are strongly dependent on the metal–adsorbate binding strength. The expanded MOF Mg_2(dobpdc) displays the same behavior upon adsorption of CO_2 and *N*,*N*′-dimethylethylenediamine. Similar sensitivity to local symmetry is expected for any open metal site, making X-ray spectroscopy an ideal tool for examining adsorption in such MOFs. Qualitative agreement between ambient-temperature experimental and 0 K theoretical spectra is good, with minor discrepancies thought to result from framework vibrational motion.

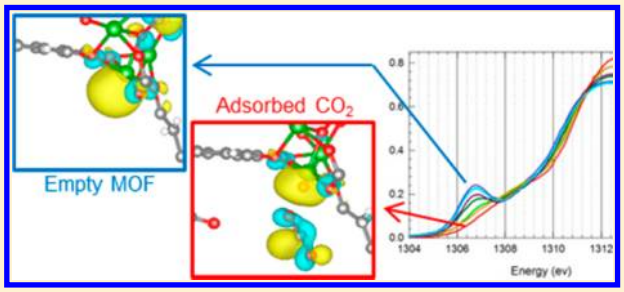

INTRODUCTION

Metal–organic frameworks (MOFs) that feature internal pore surfaces replete with open metal sites—five-coordinate metal cations known to behave as Lewis acids—are presently among the most promising solid adsorbents for selectively removing CO_2 from dry gas mixtures. Open metal sites preferentially adsorb CO_2 over N_2 or CH_4 due to its larger quadrupole moment and greater polarizability. The moderate heat of adsorption of CO_2 onto such sites produces selective, high-capacity adsorbents that can be easily regenerated via temperature or vacuum swing methods. The MOF-74 series of MOFs have been widely studied for their high performance in both gas separation and hydrogen storage applications.[1−5] In particular, Mg-MOF-74 (CPO-27-Mg, Mg_2(dobdc) (dobdc^{4-} = 2,5-dioxido-1,4-benzenedicarboxylate)) is a promising adsorbent for selective CO_2 adsorption due to its large CO_2 capacity and high selectivity for CO_2 over other gases.[6−9] This MOF features a unique five-coordinate square-pyramidal geometry around the Mg sites; unlike other square-pyramidal Mg complexes,[10,11] the organic framework in Mg-MOF-74 constrains the bond angles at the Mg sites and ensures that a significant portion of the Mg coordination sphere is available for adsorbing other species. The Mg sites can therefore be considered quasi-octahedral, with the apical site vacant. To date, characterization efforts aimed at a microscopic understanding of interactions between gases and the adsorbent have consisted primarily of low-temperature X-ray and neutron diffraction experiments,[12−14] NMR spectroscopy,[15] infrared spectroscopy,[7] inelastic neutron scattering,[16] and theoretical studies.[7,17,18] These studies have determined a tilted, end-on binding configuration for CO_2, but insight into any changes to the electronic structure of the MOF upon CO_2 adsorption have so far come solely from theoretical calculations. Experimental examination of these changes would validate theoretical predictions and provide a fundamental understanding of the binding mechanisms in this MOF.

Herein we directly observe changes in specific molecular orbitals at the Mg site in Mg-MOF-74 upon binding of CO_2 and *N*,*N*′-dimethylformamide (DMF) using near-edge X-ray absorption fine structure (NEXAFS) spectroscopy. We also examine such effects in Mg_2(dobpdc) (dobpdc^{4-} = 4,4′-dioxido-3,3′-biphenyldicarboxylate), an expanded analogue of Mg-MOF-74.[19] These measurements allow us to determine how the electronic interactions differ for different adsorbed species and for binding sites in a larger framework. The NEXAFS technique is element-specific, probing the unoccupied electronic states associated with the excited atom. It provides

Received: September 3, 2013
Published: November 13, 2013

   dx.doi.org/10.1021/ja408972f | J. Am. Chem. Soc. 2013, 135, 18183−18190

local electronic structure and coordination information due to the overlap between the core-level state and the empty final state and, for the soft X-rays used in this study, adherence to optical dipole selection rules. For systems with specific, chemically distinct binding sites such as the Mg sites in Mg-MOF-74, NEXAFS spectra provide high sensitivity to changes in the local electronic structure and coordination at the binding sites upon adsorption of gas molecules. A specially designed gas cell allows spectra to be collected under vacuum or under pressures of CO_2 as high as 100 Torr at ambient temperature, providing a direct comparison between the empty and bound Mg sites of the same MOF sample. In this study we demonstrate a strong spectral response to the unique geometry at the open metal sites in both MOFs, revealing a molecular orbital structure that is highly sensitive to adsorbed species and the strength of the interaction through its effects on local symmetry around the metal sites.

We employ plane-wave density functional theory (DFT) within the generalized gradient approximation to calculate the NEXAFS spectrum from optimized DFT structures. This approach has been used previously to calculate NEXAFS spectra for a variety of condensed-phase systems.[20−24] The DFT calculations not only provide spectra for comparison with experiment but also provide reasonable approximations to the X-ray excited electronic states, indicating how these are modified in the presence of adsorbed species. By coupling experiment and theory in this way, we are able to interpret observed spectral changes through a detailed study of the local electronic structure around the Mg atom. While photoemission studies have examined the electronic structure of gases adsorbed at metal surfaces,[25] our study is, to our knowledge, the first in situ observation of the electronic structure changes associated with gas adsorption in MOF interfaces.

EXPERIMENTAL SECTION

1. Experimental Details. *1.1. Gas Cell Design.* The gas cell design is similar to that of an ion chamber, adapted for transmission detection. The cell consists of a small cubic vacuum chamber with a specially designed flange and clamp to mount a silicon nitride membrane in the center. This membrane acts as an X-ray transmissive barrier separating any gas in the cell from the vacuum of the beamline X-ray source, as well as the substrate upon which the transmission samples are mounted (see below). A gas inlet with a valve allows introduction of CO_2 gas into the cell. There are two pumps, attached to the cell via a gate valve: a turbomolecular pumping station with dry vacuum pumps suitable for vacuum measurements and a dry scroll roughing pump suitable for measurements with gas present. A second valve allows the membrane to be bypassed when pulling vacuum so it will not burst from the pressure differential. The transmitted X-rays are detected with a GaAsP photodiode, mounted on a linear manipulator to allow the X-ray path length in the cell to be varied from 1 in. down to a few millimeters. Long path lengths are useful for gas-phase measurements, whereas it is advantageous to minimize the path length for measurements of the MOF materials to limit interference from free CO_2 gas. The housing of the photodiode was removed to allow X-ray detection. The entire cell can be sealed to ensure that activated MOF samples (i.e., samples in which all solvent is removed from the pores) are not exposed to water vapor when transporting the cell to a beamline for measurements.

1.2. Sample Preparation. The full details for the synthesis and preparation of samples are given in the Supporting Information. In brief, the synthesized MOF powder was suspended in a small amount (ca. 0.5 mL) of solvent (acetone, MeOH, or hexanes). The suspension was then deposited onto a Si_3N_4 membrane, and the solvent was allowed to evaporate, leaving a thin coating of powder on the membrane. For measurements of activated MOFs, the entire membrane with powder coating was loaded into a glass evacuation chamber and heated under vacuum to activate the MOF powder (see the Supporting Information for details on the activation procedure). Activated samples were then stored under dry nitrogen and loaded into the gas cell in a dry nitrogen glovebox to avoid exposure to water vapor before measurement.

1.3. NEXAFS Spectra. NEXAFS spectra were collected at bending magnet beamline 6.3.1 (10^{11} photons/s) at the Advanced Light Source at Lawrence Berkeley National Laboratory. The gas cell was mounted on an XY manipulator and attached to the downstream port on the beamline. Due to imperfect control of the powder sample thickness, care was taken to ensure that spectra could be meaningfully compared to one another. For a given sample, initial alignment using the Mg K-edge absorption was performed under vacuum. Once aligned, the sample was not moved again, so that all spectra were collected on the same spot on the sample with the same thickness and morphology. The first Mg K-edge NEXAFS spectrum of each sample was collected under vacuum, followed by progressively higher pressures of CO_2 gas. Finally, the gas was pumped out and the spectrum collected under vacuum again, to determine if any observed spectral changes were reversed.

To ensure proper normalization of the measured spectra, spectra of the incident X-ray beam were also collected using a blank silicon nitride membrane of 100 nm thickness under vacuum. To get the final spectra, we used the relation

$$\frac{I}{I_0} = e^{-\mu t} \tag{1}$$

where I is the intensity of the transmission spectrum, I_0 is the intensity of the direct beam spectrum, μ is the absorptivity, and t is the thickness of the sample. By solving for μt, we can estimate the apparent thickness of the sample under the assumption that it is uniformly thick. Because these powder samples are not uniformly thick, absolute intensities of different spectral features may be distorted relative to each other; therefore, we do not interpret absolute intensities in this study. Instead, we emphasize reversible spectral changes that occur when CO_2 gas is present and note that any distortions in absolute spectral intensities do not change during the measurement, as the same sample volume is always measured. Any spectral changes observed with this method must therefore arise from interactions with CO_2 gas and not from sample morphology. To generate comparable spectra for a given sample, we started with μt as a function of photon energy and subjected these spectra to a linear pre-edge baseline correction and intensity normalization necessary to account for changing gas absorption with pressure. After normalization, we rescaled the intensity to match the post-edge (1374 eV) step height observed in the baseline-corrected μt spectrum under vacuum. The intensity scale therefore provides an estimate of the apparent optical density of the sample due to the Mg sites only, without any contributions from CO_2 gas. These spectra were then compared to identify any spectral changes at the Mg sites signifying the binding of CO_2 in the materials. The photon energy was calibrated by collecting a total electron yield (TEY) spectrum of MgO, shown in Figure S2 (Supporting Information), and aligning the sharp low-energy spectral feature with that measured previously by Lindner et al.[26]

2. DFT Calculations. *2.1. Structural Relaxation.* The structural relaxation of Mg-MOF-74 and Mg_2(dobpdc) for the bare frameworks and for the frameworks in the presence of adsorbed molecules (CO_2, dimethylformamide, and *N,N′*-dimethylethylenediamine) are performed using the SIESTA package.[27,28] The vdW-DF2 functional is employed to account for long-range dispersion forces.[29] A recent work[18] shows that this approach can correctly predict the experimental heat of adsorption of CO_2 in MOFs. Norm-conserving Trouiller−Martin pseudopotentials[30] are used in these calculations. 2s and 2p electrons of C, N, and O atoms are explicitly included in the valence; for Mg, semicore electrons are considered (2s, 2p, and 3s). We use a variationally optimized[31] double-ζ polarized basis set including d orbitals for all atoms. The integration over the Brillouin zone is carried over 64 *k*-points.[32] Real space integrals are performed on a mesh with

dx.doi.org/10.1021/ja408972f | J. Am. Chem. Soc. 2013, 135, 18183−18190

a 280 Ry cutoff. For each calculation, we optimize the atomic positions of all atoms until forces are smaller than 40 meV/ Å. The relaxed structures are then used to compute NEXAFS spectra. The binding energy between the MOF at the Mg site and the different adsorbed species is computed using vdW-DF2. The CO_2 and DMF binding energies in Mg-MOF-74 are 41.3 and 108.1 kJ/mol, respectively. The Mg−O bond length is 2.33 Å for CO_2 and 2.07 Å for DMF. For Mg_2(dobpdc), the CO_2 and mmen binding energies are 39.3 and 105.8 kJ/mol, respectively, with 2.40 Å and 2.37 Å Mg−O bond lengths.

2.2. Calculated NEXAFS Spectra. Starting from the relaxed ground state structures computed using the methodology discussed in the previous section, we simulate X-ray absorption spectra (XAS) within a plane-wave pseudopotential orbital-occupancy-constrained DFT framework, employing the PBE functional.[33] We expect this functional to be adequate for computing the spectra, since the employed geometries, computed using the vdW-DF2 functional, are in good agreement with experiments.[18,34] The transition amplitudes are calculated according to Fermi's golden rule expression for the X-ray absorption cross-section:[35]

$$\sigma(\omega) = 4\pi^2\alpha_0\hbar\omega \sum_{\mathrm{f}} |M_{\mathrm{i}\to\mathrm{f}}|^2 \delta(E_{\mathrm{f}} - E_{\mathrm{i}} - \hbar\omega) \tag{2}$$

Here α_0 is the fine structure constant, $\hbar\omega$ is the energy of the absorbed photon, and $M_{\mathrm{i}\to\mathrm{f}}$ are the transition amplitudes between the initial (i) and final (f) states, with corresponding energy difference $E_{\mathrm{f}} - E_{\mathrm{i}}$. Within the electric-dipole approximation, we further approximate the transition amplitudes as effective single-particle matrix elements:

$$M_{\mathrm{i}\to\mathrm{f}} = \langle\Psi_{\mathrm{f}}|\hat{\varepsilon}\cdot\mathbf{R}|\Psi_{\mathrm{i}}\rangle \approx S\langle\psi_{\mathrm{f}}|\hat{\varepsilon}\cdot\mathbf{r}|\psi_{\mathrm{i}}\rangle \tag{3}$$

where $\hat{\varepsilon}$ is the polarization direction of the electromagnetic vector potential, $\boldsymbol{R}$ and $\boldsymbol{r}$ are the many-electron and single-electron position operators, and $\Psi_{\mathrm{i,f}}$ are the many-body initial and final states. The effective single-particle states, $\psi_{\mathrm{i,f}}$, are Kohn−Sham eigenstates of the ground and excited state self-consistent fields, respectively. In this wok, the initial state is always the 1s orbital of the Mg atom and the final states are accessible (i.e., unoccupied) Kohn−Sham eigenstates derived from a self-consistent field computed within the excited electron and core-hole (XCH) approximation for the electronic final state.[36] In this final-state-rule approach, the excited-state electron density is computed self-consistently subject to two constraints: (1) replacement of the ground-state pseudopotential of the core-excited atom in the given system with that derived from a similarly core-excited isolated atom (for the Mg K-edge we would assume an electronic configuration of $1s^1 2s^2 2p^6 3s^2 3p^1$) to model the hole and (2) the addition of one extra (excited) electron to the total number of ground-state valence electrons of this system.

Calculated spectra are computed from eq 2 with the δ function replaced by a Gaussian convolution with finite width (typically 0.3 eV). We did not make estimates of the core-hole lifetime of the Mg 1s core-excited state, which would impart a significant Lorentzian broadening to each computed transition. The sum over final states in our supercell calculations includes both electronic band indices and wave vectors (so-called *k*-point sampling of the first Brillouin zone). The spectral line shape is derived from a numerically converged sampling of eigenenergies and transition matrix elements within the first Brillouin zone. Typically this can require several *k*-points, and we reduce the computational effort of such calculations by exploiting a recently developed implementation of the Shirley interpolation scheme,[37] from which the entire Brillouin zone can be generated based only on information from the zone center ($k = 0$). In order to determine the band indices of dominant transitions in calculated spectra before convolution and neglecting *k*-point sampling, in some cases we show transition probabilities, $|M_{\mathrm{i}\to\mathrm{f}}|^2$, from the Brillouin zone center only. Similarly, to interpret such transitions, we also examine isosurfaces of the electronic component of the excited state, approximated as a Kohn−Sham eigenstate of the XCH self-consistent field at $k = 0$.

In this work, we compare Mg K-edge spectra for various MOFs with and without absorbed species or functionalization. Our approach uses pseudopotentials for efficient plane-wave representation of the valence electronic structure only. In the spirit of our ΔSCF approach, we might compute relative core-excitation energies of Mg atoms in different systems using total energy differences. However, for systems with differing periodic boundary conditions, total energies are not comparable. Instead, one should compare energies that are independent of system size, and the energy of a charge-neutral atomic excitation embedded in a condensed phase should converge, beyond a certain minimum supercell volume, to a quantity independent of the chosen periodic boundary condition. However, our use of pseudopotentials prevents us from computing meaningful energy differences between excited and ground states, since the addition of a modified pseudopotential to the excited state system adds an unknown shift to the total energy. Instead, we make comparison to a theoretical standard—the isolated excited- and ground-state atom under the same periodic boundary conditions.[23] This is equivalent to computing a difference in formation energies between the excited and ground states, and formation energies are numerically well-defined within a pseudopotential framework.[22] In practice, we then align the computed spectrum of a well-defined system (MgO in this case) to experiment and use the same constant of alignment in all further calculations using the same excited-state pseudopotential for Mg.

To analyze and interpret our simulated XAS, we imagine the K-edge excitonic excited states to be factorizable into a product of the 1s hole state and the corresponding electronic states of energy greater than or equal to that of the highest occupied state of the XCH self-consistent field. We plot representations of these electronic states as isosurfaces in 3D space and explore their symmetry and hybridization in the vicinity of the excited Mg atom, in order to correlate specific spectral changes with specific adsorption interactions.

RESULTS AND DISCUSSION

1. NEXAFS Spectra. NEXAFS spectra at the Mg K-edge were collected for Mg-MOF-74 in its activated form and for the same sample in contact with CO_2 gas at various pressures. The spectrum of DMF-ligated Mg-MOF-74 (DMF = *N*,*N*′-dimethylformamide) was also collected to explore the spectral dependence on the different strengths of adsorption interactions for different adsorbed species at the Mg site. DMF is used as a solvent during synthesis of the MOF and interacts strongly with the Mg site, whereas the Mg−CO_2 interaction is weaker. We also performed CO_2 adsorption measurements for Mg_2(dobpdc) (dobpdc^{4-} = 4,4′-dioxido-3,3′-biphenyldicarboxylate),[19] an expanded analogue to Mg-MOF-74, to explore possible differences in the adsorption interactions in the two MOFs (see the Supporting Information for Mg_2(dobpdc) data). While the local Mg environment is similar, Mg_2(dobpdc) has longer organic linkers, allowing us to examine how the linkers and overall framework structure affect the electronic interactions at the binding sites. Mg_2(dobpdc) was originally synthesized to facilitate functionalization with *N*,*N*′-dimethylethylenediamine (mmen), which further increases CO_2 adsorption efficiency.[19,38] We collected Mg K-edge spectra of the functionalized form mmen-Mg_2(dobpdc) to compare the electronic interactions of CO_2 and mmen with the Mg sites in this MOF. Like DMF, mmen interacts strongly with the Mg site and provides a useful contrast to the weaker interaction with CO_2. Finally, we collected the NEXAFS spectrum of cubic MgO for energy calibration and for assistance in the interpretation of observed spectral changes.

A representative series of spectra for one of the Mg-MOF-74 samples is shown in Figure 1a. A distinct pre-edge peak is observed for the activated sample that is suppressed and blue-shifted when CO_2 gas is introduced, accompanied by an increase in intensity and slight blue shift of the strongest main edge feature. These features evolve progressively as a function of gas pressure. The nonzero experimental pressures span

dx.doi.org/10.1021/ja408972f | J. Am. Chem. Soc. 2013, 135, 18183−18190

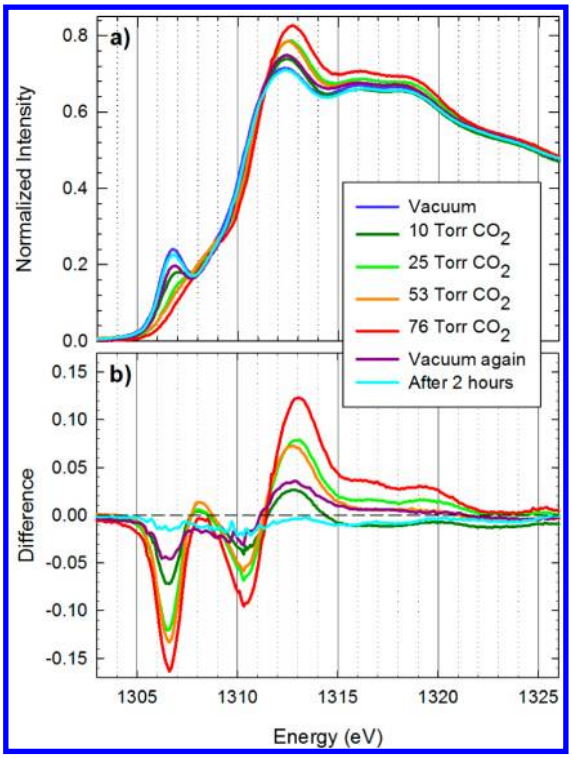

Figure 1. (a) Mg K-edge spectra of Mg-MOF-74 under vacuum, with increasing CO_2 gas pressures, under vacuum again after pumping the gas out, and a final spectrum collected 2 h later. The spectra taken with gas correspond to ~0.28, ~ 0.46, ~0.57 and ~0.65 CO_2 molecules per Mg site, in order of increasing pressure. All spectra were collected at an ambient temperature of 295 K. (b) Difference spectra generated by subtracting the initial vacuum spectrum from all subsequent spectra.

~0.28 to ~0.65 CO_2 molecules per Mg site, according to adsorption isotherm data.[1] When the gas is pumped out, the spectral changes reverse, with the pre-edge feature reappearing within minutes and nearly full reversion to the original vacuum spectrum after 2 h. Figure 1b shows the difference spectra generated by subtracting the initial vacuum spectrum from each subsequent spectrum. The two negative regions at lower energy correspond to the suppression of the pre-edge peak and blue shift of the main edge absorption onset upon gas adsorption, while the broad positive region at higher energy corresponds to the increased intensity in the main edge features upon adsorption. The integral under some of the difference curves in Figure 1b is effectively 0, consistent with the dipole oscillator sum rule prediction that observed spectral changes result from redistribution of Mg 3p spectral weight as the Mg environment changes, as discussed below. Since only ~65% of the Mg sites are occupied at 76 Torr, the spectrum of the fully saturated MOF can be approximated by subtracting a percentage of the vacuum spectrum from the 76 Torr spectrum, as shown in Figure 2. The result clearly lacks the pre-edge peak that appears at 1306.6 eV for the activated MOF.

Similar spectral changes are observed when other molecules are adsorbed in the MOF. Figure 3a shows the Mg K-edge spectra for activated Mg-MOF-74, Mg-MOF-74 in 76 Torr CO_2, and DMF-ligated Mg-MOF-74. Difference spectra are shown in Figure 3b. In the DMF case we expect the Mg sites to be fully saturated. The pre-edge shows a very broad, weak shoulder that extends to lower energy, but the changes in the main edge absorption onset and main edge intensity are very

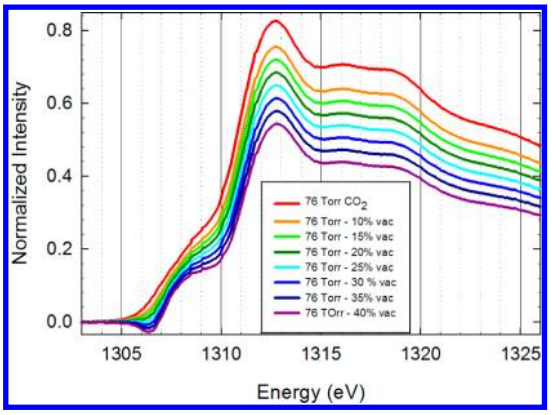

Figure 2. Mg K-edge NEXAFS spectrum of Mg-MOF-74 in 76 Torr CO_2 gas and the same spectrum with various percentages of the vacuum spectrum subtracted. These spectra therefore approximate the shape of the spectrum of Mg-MOF-74 on saturatation with CO_2 gas. Note the absence of the prepeak at 1306.6 eV that is characteristic of the empty Mg binding sites.

similar to those of the CO_2 case. The pre-edge peak is absent when CO_2 or DMF is present, indicating that it is associated with the coordinatively unsaturated Mg sites in the activated MOF. Similar pre-edge features have been observed for other metal K-edges of crystalline solids and theorized to arise when local symmetry around the metal site is broken by thermal motion, leading to mixing of some metal p character into the predominantly metal s character of the lowest energy excitations at that site.[39−44] Core-excited states comprising a 1s hole and local electronic s character at the same site are inaccessible in NEXAFS due to the dipole selection rule. Valid for optical excitations with low momentum transfer, the selection rule permits electronic transitions with an associated change in angular momentum of ±1. However, the s−p mixing induced by broken symmetry renders these low-energy excited states optically active and evident as pre-edge features in the NEXAFS spectrum. The unique and highly anisotropic square-pyramidal geometry at the Mg sites in activated Mg-MOF-74 induces similar, but much more pronounced, mixing of Mg 3p and 3s character in the low-energy excited states, resulting in strong pre-edge X-ray absorption, as we observe. The suppression of the pre-edge peak upon adsorption of CO_2 and DMF can therefore be explained via a partial restoration of octahedral symmetry around the Mg sites in the MOF.

This interpretation is confirmed using DFT calculations to directly examine the Mg 1s core-excited states in the MOF and their contributions to the NEXAFS spectrum. Calculated NEXAFS spectra for the three experimental cases for Mg-MOF-74 are shown in Figure 3c, along with the transition probabilities from which the spectra were generated. Difference spectra are shown in Figure 3d. The intensity of a given transition is dependent not only on the overlap between the empty final excited state and the Mg 1s orbital but also on the degree of p character of the final state within this overlap. Final states that are highly delocalized or have low p character at the Mg site will have weak transition probabilities.

We find generally good agreement between experimental and calculated spectra. Spectral features are reproduced at the correct energies, and the spectral changes upon gas adsorption—including the suppression of the pre-edge peak, blue shift of the main edge onset, and increased intensity and blue shift of the main edge features—are reproduced as well.

dx.doi.org/10.1021/ja408972f | J. Am. Chem. Soc. 2013, 135, 18183−18190

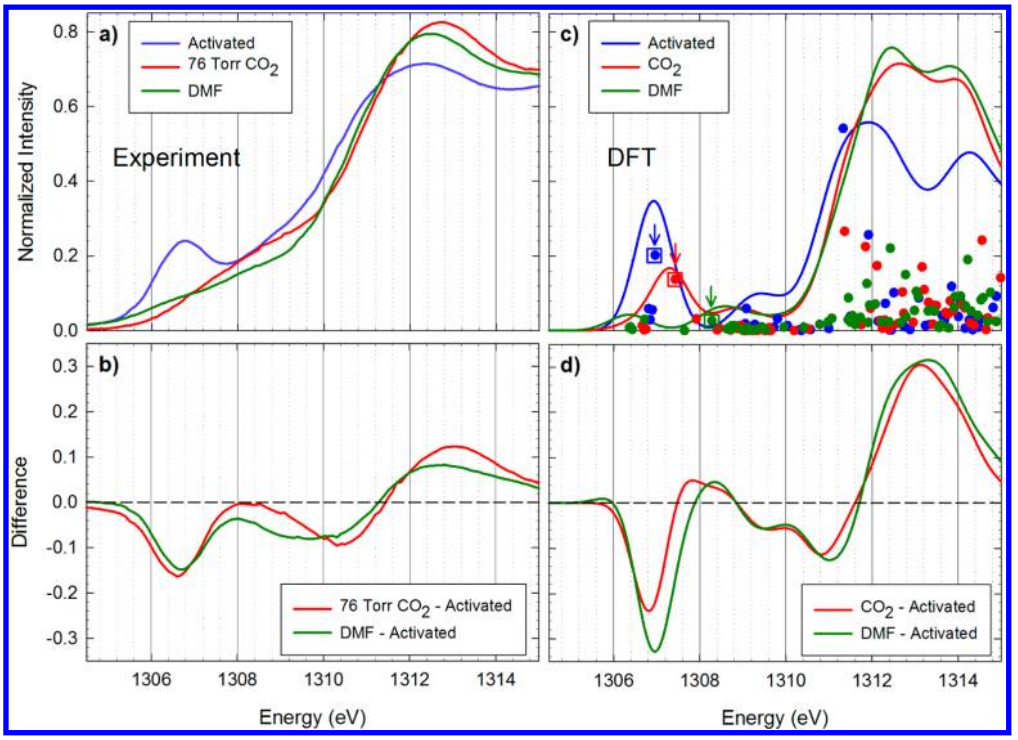

Figure 3. (a) NEXAFS spectra for activated Mg-MOF-74 (blue), Mg-MOF-74 with 76 Torr CO_2 (red), and Mg-MOF-74 with DMF solvent (green). (b) Difference spectra generated by subtracting the activated MOF spectrum from the 76 Torr CO_2 (red) and DMF (green) spectra. (c) Calculated NEXAFS spectra (lines) for activated Mg-MOF-74 (blue), Mg-MOF-74 with adsorbed CO_2 (red), and DMF ligated Mg-MOF-74 (green), along with the transition probabilities (circles) used to generate the spectra, corresponding to individual excited states. Only the transitions to states at the Brillouin zone center (k = 0) are shown. The intensity of the pre-edge features is dominated by a single transition in each case, marked with a colored square and arrow. (d) Difference spectra generated by subtracting the computed activated MOF spectrum from the computed adsorbed CO_2 (red) and computed DMF ligated (green) spectra.

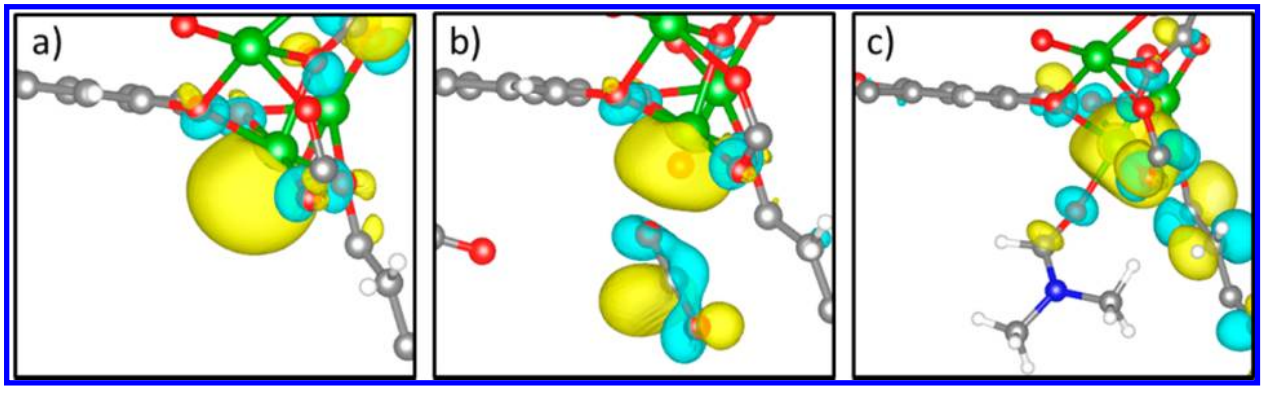

Figure 4. (a) Excited state wave function corresponding to the blue marked transition in Figure 3c. Magnesium atoms are shown in green, oxygen atoms in red, carbon atoms in gray, and hydrogen atoms in white. The two phases of the wave function are shown in yellow and teal. (b) Excited state wave function corresponding to the red marked transition in Figure 3c. (c) Excited state wave function corresponding to the green marked transition in Figure 3c. While these electronic states extend to neighboring linker and ligand molecules, the spectral features given by the calculation sample these states only near the Mg nucleus.

Minor discrepancies likely arise from the effects of thermal motion in the ambient-temperature experimental spectra; computed spectra use 0 K structures. For example, the pre-edge peak is much more intense in the computed spectra, especially when CO_2 is adsorbed. Previous studies of condensed-phase systems have shown that the lower-energy spectral features are more sensitive to thermal broadening;[45] these low-energy states are highly localized and resemble molecular states with appropriately high sensitivity to atomic positions, whereas higher-energy features resemble bands that are less sensitive to these positions. The combination of CO_2 adsorption and thermal broadening in Mg-MOF-74 could therefore reduce the intensity of the pre-edge peak until it is no longer observable.

The importance of dynamics for adsorbed CO_2 in Mg-MOF-74 at ambient temperature has been demonstrated previously,[15] so it is possible that the thermal motion of the adsorbed CO_2 itself affects the spectrum. To approximate this, we applied a series of translations and rotations to the adsorbed CO_2 and computed the spectral sensitivity to these motions (see Figure S4 for details). Clear changes in both the pre-edge and main edge regions of the spectrum appear, but the Boltzmann-

dx.doi.org/10.1021/ja408972f | J. Am. Chem. Soc. 2013, 135, 18183−18190

weighted average yields a spectrum that is indistinguishable from the zero-Kelvin spectrum. This suggests that the NEXAFS spectrum is primarily sensitive to thermal motion of the framework itself rather than of the adsorbed species.

2. X-ray Excited-State Analysis. Given the qualitative agreement between experiment and theory, a closer examination of the excited electronic states associated with the computed transitions provides further insight into the origin of the pre-edge peak. For activated Mg-MOF-74, the intensity in the pre-edge region arises primarily from a single transition, marked in Figure 3c and with the corresponding excited state wave function shown in Figure 4a. This excited state has a clear contribution from the Mg 3s orbital and, as such, should be inaccessible in NEXAFS. In the activated MOF, the state extends into the unoccupied apical site and is no longer centered on the Mg nucleus, which implies a nonzero first moment with respect to the Mg 1s core orbital and hence an allowed optical transition. The other empty states in the pre-edge region also feature this localized, distorted lobe at the Mg site but have stronger hybridization with the π systems on the ligands, delocalizing the states, which reduces overlap with the core orbital and lowers transition intensities. When CO_2 is adsorbed in the MOF, the pre-edge feature is once again dominated by a single transition. The corresponding final state wave function is shown in Figure 4b. It looks similar to the most intense state in the activated MOF, again showing a localized, distorted lobe at the Mg site, but now there is clear hybridization between this lobe and the π^* orbital of the adsorbed CO_2 molecule. While the adsorbed CO_2 does not appreciably restore spherical symmetry at the Mg site, the intensity of the transition is reduced because the hybridization with the CO_2 molecule delocalizes the state.

When DMF coordinates to the Mg site, the two low-intensity features in the pre-edge region each have a dominant transition. The low-energy transition corresponds to a state consisting primarily of the π^* orbital of the DMF molecule, showing very slight hybridization with the distorted lobe at the Mg site. The high-energy transition, marked in Figure 3c and with the corresponding wave function shown in Figure 4c, shows a less distorted lobe that is now centered on the Mg. The DMF molecule partially restores the octahedral symmetry around the Mg and the spherical symmetry of the empty electronic state, reducing the intensity of the NEXAFS transition. The dipole moment and larger polarizability of DMF with respect to CO_2 result in a larger binding energy and shorter bond length, as reported in the Experimental Section. This indicates that strongly interacting species will have more pronounced spectral signatures upon adsorption at open metal sites. While adsorbed CO_2 and DMF are distinct in the computed spectra, they are more difficult to distinguish experimentally, implying that thermal motion may mask some of the spectral signatures for different adsorbed species.

Measurements of Mg_2(dobpdc) show similar, but less pronounced, pre-edge behavior (see the Supporting Information for details). This indicates that the pre-edge feature is a general phenomenon that will appear whenever there is a change in local symmetry at Mg sites in a material. To test this, we computed the NEXAFS spectrum of octahedral MgO as well as two distorted cases, in which the bond length of the apical oxygen was increased by 0.5 and 1.0 Å. The results are shown in Figure 5. For octahedral MgO, some low-energy transitions have little or no intensity in the spectrum, consistent with previous studies of MgO.[26,46] The final state wave functions for these transitions resemble the case of DMF-ligated Mg-MOF-74 in Figure 4c, consisting primarily of the empty Mg 3s orbital centered on the Mg site (see Figure S5 in the Supporting Information for the MgO wave functions). When the apical oxygen bond length is increased, spectral features similar to those observed for Mg-MOF-74 appear. In particular, we find a distinct new pre-edge feature which arises from an asymmetric, distorted electronic state around the Mg that resembles that seen for activated Mg-MOF-74 (Figure 4a). Further increasing the MgO bond length creates a more dramatic modification of the pre-edge. This confirms that breaking the octahedral symmetry at the Mg site creates the spectral features observed for Mg-MOF-74, and the spectral sensitivity to the Mg–O bond length in MgO underscores the importance of framework dynamics in spectral modeling.

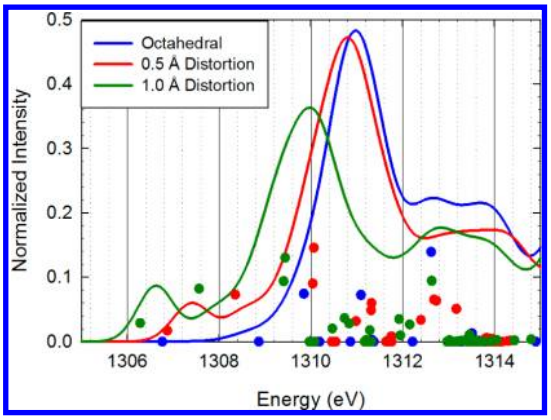

Figure 5. Calculated NEXAFS spectra for octahedral MgO, MgO in which the Mg–O bond distance of the apical oxygen has been increased by 0.5 Å, and MgO in which the Mg–O bond distance of the apical oxygen has been increased by 1.0 Å. Also shown are the transition probabilities corresponding to γ point states, which form the lower bound of any spectral feature in the simulated spectrum. Note that the low-energy transitions for octahedral MgO have zero intensity due to the octahedral symmetry. With distortions to the apical oxygen, these transitions become active in the spectrum, creating a new pre-edge peak.

CONCLUSION

We find strong sensitivity of the Mg K-edge NEXAFS spectrum to the adsorption of CO_2 gas and DMF in Mg-MOF-74 and to adsorption of CO_2 gas and mmen in Mg_2(dobpdc). The open coordination at the Mg sites in these materials activates otherwise forbidden transitions in the NEXAFS spectrum, creating pre-edge features that are signatures of the open metal sites. While all of the adsorbed species reduce the intensity of these pre-edge features, we find that more strongly adsorbed molecules result in a more octahedral-like geometry around the Mg and a stronger spectral signature. This detailed and direct information about the electronic structure and interactions at the active Mg sites fills a critical gap in validating empirical, experimental, and theoretical models for the fundamental gas interaction mechanisms in these materials. We find good agreement between our ambient-temperature measurements and DFT calculations based on static structures, with minor discrepancies that are likely due to vibrational motion in the framework which instantaneously modifies the symmetry at the Mg sites.

The high spectral sensitivity to the Mg site symmetry underscores the versatility of NEXAFS for in situ gas

dx.doi.org/10.1021/ja408972f | J. Am. Chem. Soc. 2013, 135, 18183–18190

adsorption measurements in nanoporous materials such as MOFs, especially those with chemically distinct open metal sites. NEXAFS can also probe adsorption occurring at the organic linkers or functional additives in MOFs, to explore more complex adsorption interactions. This approach provides a new method to monitor the chemistry within working MOFs with chemical specificity that will be useful to test theoretical models for structure, chemistry, and potentially dynamics and kinetics. Its systematic application may inform the design of MOFs with improved performance in specific tasks.

■ ASSOCIATED CONTENT

Supporting Information

Text and figures giving synthetic details and sample preparation, adsorption isotherms, NEXAFS spectra and DFT calculations of MgO with and without apical distortion, NEXAFS spectra and DFT calculations of Mg_2(dobpdc). This material is available free of charge via the Internet at http://pubs.acs.org.

■ AUTHOR INFORMATION

Corresponding Author

jbkortright@lbl.gov

Author Contributions

All authors have given approval to the final version of the manuscript.

Notes

The authors declare no competing financial interest.

■ ACKNOWLEDGMENTS

This work was supported by the Center for Gas Separations Relevant to Clean Energy Technologies, an Energy Frontier Research Center funded by the U.S. Department of Energy, Office of Science, Office of Basic Energy Sciences, under Award Number DE-SC0001015. Portions of this work were performed as User Projects at the Advanced Light Source and Molecular Foundry, both at Lawrence Berkeley National Laboratory and supported by the Office of Science, Office of Basic Energy Sciences, of the U.S. Department of Energy under Contract No. DE-AC02-05CH11231. Calculations used LBNL Lawrencium, the National Energy Research Scientific Computing Center, LBNL, and the Molecular Foundry computing resources nano and vulcan, managed by the High Performance Computing Services Group, LBNL.

■ REFERENCES

(1) Caskey, S. R.; Wong-Foy, A. G.; Matzger, A. J. *J. Am. Chem. Soc.* **2008**, *130*, 10870.

(2) Dietzel, P. D. C.; Besikiotis, V.; Blom, R. *J. Mater. Chem.* **2009**, *19*, 7362.

(3) Herm, Z. R.; Swisher, J. A.; Smit, B.; Krishna, R.; Long, J. R. *J. Am. Chem. Soc.* **2011**, *133*, 5664.

(4) Herm, Z. R.; Krishna, R.; Long, J. R. *Microporous Mesoporous Mater.* **2012**, *151*, 481.

(5) Yu, D.; Yazaydin, A. O.; Lane, J. R.; Dietzel, P. D. C.; Snurr, R. Q. *Chem. Sci.* **2013**, *4*, 3544.

(6) Britt, D.; Furukawa, H.; Wang, B.; Glover, T. G.; Yaghi, O. M. *Proc. Natl. Acad. Sci. U.S.A.* **2009**, *106*, 20637.

(7) Valenzano, L.; Civalleri, B.; Chavan, S.; Palomino, G. T.; Arean, C. O.; Bordiga, S. *J. Phys. Chem. C* **2010**, *114*, 11185.

(8) Bao, Z.; Yu, L.; Ren, Q.; Lu, X.; Deng, S. *J. Colloid Interface Sci.* **2011**, *353*, 549.

(9) Mason, J. A.; Sumida, K.; Herm, Z. R.; Krishna, R.; Long, J. R. *Energy Environ. Sci.* **2011**, *4*, 3030.

(10) Wong, A.; Ida, R.; Mo, X.; Gan, Z.; Poh, J.; Wu, G. *J. Phys. Chem. A* **2006**, *110*, 10084.

(11) Guzei, I. A.; McGaff, R. W.; Kieler, H. M. *Acta Crystallogr., Sect. C: Cryst. Struct. Commun.* **2005**, *61*, M472.

(12) Dietzel, P. D. C.; Johnsen, R. E.; Fjellvag, H.; Bordiga, S.; Groppo, E.; Chavan, S.; Blom, R. *Chem. Commun.* **2008**, 5125.

(13) Wu, H.; Simmons, J. M.; Srinivas, G.; Zhou, W.; Yildirim, T. *J. Phys. Chem. Lett.* **2010**, *1*, 1946.

(14) Queen, W. L.; Brown, C. M.; Britt, D. K.; Zajdel, P.; Hudson, M. R.; Yaghi, O. M. *J. Phys. Chem. C* **2011**, *115*, 24915.

(15) Kong, X.; Scott, E.; Ding, W.; Mason, J. A.; Long, J. R.; Reimer, J. A. *J. Am. Chem. Soc.* **2012**, *134*, 14341.

(16) Sumida, K.; Brown, C. M.; Herm, Z. R.; Chavan, S.; Bordiga, S.; Long, J. R. *Chem. Commun.* **2011**, *47*, 1157.

(17) Valenzano, L.; Civalleri, B.; Sillar, K.; Sauer, J. *J. Phys. Chem. C* **2011**, *115*, 21777.

(18) Poloni, R.; Smit, B.; Neaton, J. B. *J. Phys. Chem. A* **2012**, *116*, 4957.

(19) McDonald, T. M.; Lee, W. R.; Mason, J. A.; Wiers, B. M.; Hong, C. S.; Long, J. R. *J. Am. Chem. Soc.* **2012**, *134*, 7056.

(20) Shih, O.; England, A. H.; Dallinger, G. C.; Smith, J. W.; Duffey, K. C.; Cohen, R. C.; Prendergast, D.; Saykally, R. J. *J. Chem. Phys.* **2013**, *139*, 035104.

(21) Zegkinoglou, I.; Ragoussi, M.-E.; Pemmaraju, C. D.; Johnson, P. S.; Pickup, D. F.; Ortega, J. E.; Prendergast, D.; de la Torre, G.; Himpsel, F. J. *J. Phys. Chem. C* **2013**, *117*, 13357.

(22) Jiang, P.; Prendergast, D.; Borondics, F.; Porsgaard, S.; Giovanetti, L.; Pach, E.; Newberg, J.; Bluhm, H.; Besenbacher, F.; Salmeron, M. *J. Chem. Phys.* **2013**, *138*, 024704.

(23) England, A. H.; Duffin, A. M.; Schwartz, C. P.; Uejio, J. S.; Prendergast, D.; Saykally, R. J. *Chem. Phys. Lett.* **2011**, *514*, 187.

(24) Schwartz, C. P.; Uejio, J. S.; Duffin, A. M.; England, A. H.; Kelly, D. N.; Prendergast, D.; Saykally, R. J. *Proc. Natl. Acad. Sci. U.S.A.* **2010**, *107*, 14008.

(25) Wyrick, J.; Kim, D.-H.; Sun, D.; Cheng, Z.; Lu, W.; Zhu, Y.; Berland, K.; Kim, Y. S.; Rotenberg, E.; Luo, M.; Hyldgaard, P.; Einstein, T. L.; Bartels, L. *Nano Lett.* **2011**, *11*, 2944.

(26) Lindner, T.; Sauer, H.; Engel, W.; Kambe, K. *Phys. Rev. B* **1986**, *33*, 22.

(27) Soler, J. M.; Artacho, E.; Gale, J. D.; Garcia, A.; Junquera, J.; Ordejon, P.; Sanchez-Portal, D. *J. Phys.: Condens. Matter* **2002**, *14*, 2745.

(28) Roman-Perez, G.; Soler, J. M. *Phys. Rev. Lett.* **2009**, *103*, 096103.

(29) Lee, K.; Murray, E. D.; Kong, L.; Lundqvist, B. I.; Langreth, D. C. *Phys. Rev. B* **2010**, *82*, 081101.

(30) Troullier, N.; Martins, J. L. *Phys. Rev. B* **1991**, *43*, 1993.

(31) Junquera, J.; Paz, O.; Sanchez-Portal, D.; Artacho, E. *Phys. Rev. B* **2001**, *64*, 235111.

(32) Moreno, J.; Soler, J. M. *Phys. Rev. B* **1992**, *45*, 13891.

(33) Perdew, J. P.; Burke, K.; Ernzerhof, M. *Phys. Rev. Lett.* **1996**, *77*, 3865.

(34) Rohrer, J.; Hyldgaard, P. *Phys. Rev. B* **2011**, *83*, 165423.

(35) Stöhr, J. *NEXAFS Spectroscopy*; Springer: New York, 1992.

(36) Prendergast, D.; Galli, G. *Phys. Rev. Lett.* **2006**, *96*, 215502.

(37) Prendergast, D.; Louie, S. G. *Phys. Rev. B* **2009**, *80*, 235126.

(38) Planas, N.; Dzubak, A. L.; Poloni, R.; Lin, L.-C.; McManus, A.; McDonald, T. M.; Neaton, J. B.; Long, J. R.; Smit, B.; Gagliardi, L. *J. Am. Chem. Soc.* **2013**, *135*, 7402.

(39) Pascal, T. A.; Boesenberg, U.; Richardson, T. J.; Weng, T.-C.; Sokaras, D.; Nordlund, D.; McDermott, E.; Moewes, A.; Cabana, J.; Prendergast, D. G. *J. Chem. Phys.* **2013**, accepted for publication.

(40) Manuel, D.; Cabaret, D.; Brouder, C.; Sainctavit, P.; Bordage, A.; Trcera, N. *Phys. Rev. B* **2012**, *85*, 224108.

(41) Pantelides, S. T. *Phys. Rev. B* **1975**, *11*, 2391.

(42) Kunz, A. B. *Phys. Rev. B* **1975**, *12*, 5890.

(43) Pantelides, S. T.; Brown, F. C. *Phys. Rev. Lett.* **1974**, *33*, 298.

(44) Kunz, A. B.; Collins, T. C.; Devreese, J. T. *J. Phys. Part C: Solid State Phys.* **1972**, *5*, 3259.

(45) Schwartz, C. P.; Uejio, J. S.; Duffin, A. M.; England, A. H.; Prendergast, D.; Saykally, R. J. *J. Chem. Phys.* **2009**, *131*, 114509.
(46) Mizoguchi, T.; Tanaka, I.; Yoshiya, M.; Oba, F.; Ogasawara, K.; Adachi, H. *Phys. Rev. B* **2000**, *61*, 2180.